



Cite this: *CrystEngComm*, 2022, 24, 7292

Evaluating solvothermal and mechanochemical routes towards the metal–organic framework $\text{Mg}_2(m\text{-dobdc})^\ddagger$

Elena Y. Chen,[†] Ruth M. Mandel[†] and Phillip J. Milner^{*}

Metal–organic frameworks bearing coordinatively unsaturated $\text{Mg}(\text{II})$ sites are promising materials for gas storage, chemical separations, and drug delivery due to their low molecular weights and lack of toxicity. However, there remains a limited number of such MOFs reported in the literature. Herein, we investigate the gas sorption properties of the understudied framework $\text{Mg}_2(m\text{-dobdc})$ ($\text{dobdc}^{4-} = 4,6\text{-dioxido-1,3-benzenedicarboxylate}$) synthesized under both solvothermal and mechanochemical conditions. Both materials are found to be permanently porous, as confirmed by 77 K N_2 adsorption measurements. In particular, $\text{Mg}_2(m\text{-dobdc})$ synthesized under mechanochemical conditions using exogenous organic base displays one of the highest capacities reported to date (6.14 mmol g^{-1}) for CO_2 capture in a porous solid under simulated coal flue gas conditions (150 mbar, 40 °C). As such, mechanochemically synthesized $\text{Mg}_2(m\text{-dobdc})$ represents a promising new framework for applications requiring high gas adsorption capacities in a porous solid.

Received 28th May 2022,
Accepted 30th June 2022

DOI: 10.1039/d2ce00739h

rsc.li/crystengcomm

Introduction

Metal–organic frameworks (MOFs) are porous, crystalline extended solids that consist of inorganic metal nodes or secondary building units (SBUs) bridged by polytopic organic linkers.¹ Their uniquely modular structures coupled with high internal surface areas have enabled numerous applications in drug delivery, catalysis, chemical separations, and gas storage.^{2–5} Frameworks containing coordinatively unsaturated metal centers, also known as open-metal site MOFs, have been extensively studied due to their ability to strongly interact with guest molecules.⁶ In particular, the canonical $\text{M}_2(\text{dobdc})$ ($\text{M} = \text{Mg}, \text{Mn}, \text{Fe}, \text{Co}, \text{Ni}, \text{Cu}, \text{Zn}, \text{Cd}$; $\text{dobdc}^{4-} = 2,5\text{-dioxido-1,4-dicarboxylate}$), MOF-74, or CPO-27 family of frameworks features hexagonal one-dimensional channels decorated with a high density of exposed $\text{M}(\text{II})$ centers (Fig. 1, left).⁷ Among the reported isostructural metal variants, the Mg analogue, $\text{Mg}_2(\text{dobdc})$, is particularly promising due to its low cost, lack of toxicity, and high gravimetric and volumetric adsorption capacities for a range of adsorbates.^{8–12} As such, the identification of new porous frameworks bearing accessible $\text{Mg}(\text{II})$ sites is highly desirable.

A closely related family of frameworks, $\text{M}_2(m\text{-dobdc})$ ($\text{M} = \text{Mg}, \text{Mn}, \text{Fe}, \text{Co}, \text{Ni}$; $m\text{-dobdc}^{4-} = 4,6\text{-dioxido-1,3-benzenedicarboxylate}$), have been reported to possess an even higher density of exposed cationic sites than MOF-74 materials due to slight differences in the ligand field around the metal center.¹³ However, $\text{Mg}_2(m\text{-dobdc})$ prepared under solvothermal conditions was initially reported to be non-porous due to difficulties associated with removing coordinating solvents such as N,N -dimethylformamide (DMF)



Fig. 1 Structures of $\text{M}_2(\text{dobdc})$ ($\text{M} = \text{Mg}, \text{Mn}, \text{Fe}, \text{Co}, \text{Ni}, \text{Cu}, \text{Zn}$; $\text{dobdc}^{4-} = 2,5\text{-dioxido-1,4-dicarboxylate}$, left) and $\text{M}_2(m\text{-dobdc})$ ($\text{M} = \text{Mg}, \text{Mn}, \text{Fe}, \text{Co}, \text{Ni}$; $m\text{-dobdc}^{4-} = 4,6\text{-dioxido-1,3-dicarboxylate}$, right). Green, gray, white, and red spheres correspond to magnesium, carbon, hydrogen, and oxygen, respectively.

Department of Chemistry and Chemical Biology, Cornell University, Ithaca, NY 14850, USA. E-mail: pjm347@cornell.edu

[†] Electronic supplementary information (ESI) available: All procedures and characterization data. See DOI: <https://doi.org/10.1039/d2ce00739h>

[‡] Contributed equally.

or methanol (MeOH) from the framework pores.¹³ Although $\text{Mg}_2(m\text{-dobdc})$ was later reported to be porous when prepared under mechanochemical conditions,¹⁴ much about its intrinsic gas sorption properties, such as the accessibility of the $\text{Mg}(\text{II})$ sites to guest molecules,⁸ remains relatively unknown.

Herein, we systematically investigate the synthesis and gas sorption properties of fully desolvated $\text{Mg}_2(m\text{-dobdc})$. Careful washing and activation of $\text{Mg}_2(m\text{-dobdc})$ prepared under traditional solvothermal (ST) conditions, termed $\text{Mg}_2(m\text{-dobdc})\text{-ST}$, enables access to a material with a similar 77 K N_2 Brunauer–Emmett–Teller (BET) surface area as closely related $\text{Mg}_2(\text{dobdc})$. In addition, we report an improved mechanochemical (MC) method to reliably prepare $\text{Mg}_2(m\text{-dobdc})\text{-MC}$ using exogenous organic base.¹⁴ Beyond the inherent advantages in scalability and waste minimization offered by mechanochemical syntheses,^{15–17} $\text{Mg}_2(m\text{-dobdc})\text{-MC}$ exhibits higher gas adsorption capacities than $\text{Mg}_2(m\text{-dobdc})\text{-ST}$. Indeed, at 150 mbar of CO_2 and 40 °C, conditions relevant to CO_2 capture from coal flue gas,¹⁸ $\text{Mg}_2(m\text{-dobdc})\text{-MC}$ exhibits an higher CO_2 uptake (6.14 mmol g^{-1}) than even $\text{Mg}_2(\text{dobdc})$ (5.28 mmol g^{-1}).^{12,19} This represents one of the highest capacities reported to date for CO_2 capture in a porous solid under simulated coal flue gas conditions.²⁰ Overall, our findings suggest that $\text{Mg}_2(m\text{-dobdc})$ prepared under mechanochemical conditions represents a promising and scalable alternative to ubiquitous $\text{Mg}_2(\text{dobdc})$ for applications in chemical separations, gas storage, and beyond.

Results and discussion

We commenced our studies into the synthesis and gas sorption properties of $\text{Mg}_2(m\text{-dobdc})$ by optimizing the synthesis of $\text{H}_4m\text{-dobdc}$ (Fig. 2). In our hands, the previously reported synthesis of $\text{H}_4m\text{-dobdc}$ from resorcinol *via* the Kolbe–Schmitt reaction was only modestly reproducible, often yielding the monocarboxylic acid **1** instead of $\text{H}_4m\text{-dobdc}$ (Fig. 2). Two modifications to the standard preparation were identified to make the synthesis of $\text{H}_4m\text{-dobdc}$ more reliable (see ESI† section 2 for details). First, starting from commercially available **1** in place of resorcinol improved the reproducibility of the reaction, likely because only a single carboxylation reaction must take place to yield $\text{H}_4m\text{-dobdc}$.²¹ Second, the reaction temperature (250 °C) was found to be a critical parameter and best monitored using an internal thermocouple placed directly in the solvent-free reaction mixture. With these modifications in place, we were able to reliably synthesize $\text{H}_4m\text{-dobdc}$ on >5 g scale in a single batch.

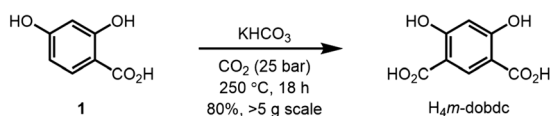


Fig. 2 Synthesis of $\text{H}_4m\text{-dobdc}$ from **1**.

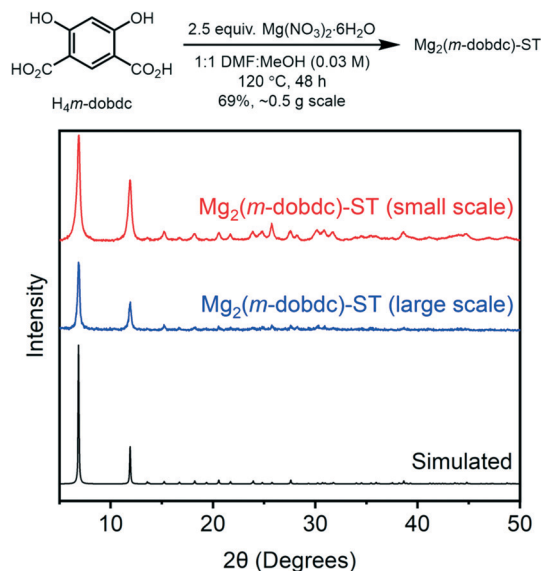


Fig. 3 PXRD ($\lambda = 1.5406 \text{ \AA}$) patterns of $\text{Mg}_2(m\text{-dobdc})\text{-ST}$ synthesized on small and large scale under solvothermal conditions. The simulated pattern based on the previously reported single-crystal X-ray diffraction structure of the isostructural framework $\text{Co}_2(m\text{-dobdc})$ is included for reference.²⁵

The previously reported small-scale solvothermal synthesis of $\text{Mg}_2(m\text{-dobdc})$ employed $\text{Mg}(\text{NO}_3)_2 \cdot 6\text{H}_2\text{O}$ as the Mg precursor in 2 : 1 DMF : MeOH at 120 °C.¹³ In order to identify the optimal solvothermal conditions for preparing $\text{Mg}_2(m\text{-dobdc})$, several combinations of amide (DMF or *N,N*-dimethylacetamide) and alcohol (MeOH, ethanol, H_2O) solvents were evaluated (ESI† Table S1, see ESI† section 3 for details). Other methods previously reported for the

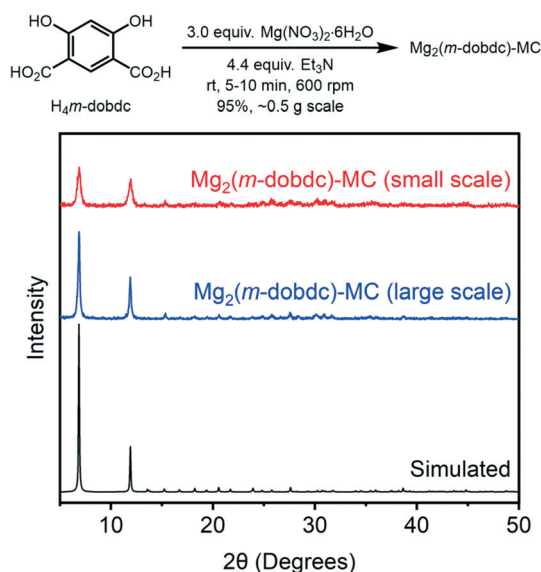


Fig. 4 PXRD ($\lambda = 1.5406 \text{ \AA}$) patterns of $\text{Mg}_2(m\text{-dobdc})\text{-MC}$ synthesized on small and large scale under mechanochemical conditions. The simulated pattern based on the previously reported single-crystal X-ray diffraction structure of the isostructural framework $\text{Co}_2(m\text{-dobdc})$ is included for reference.²⁵



Fig. 5 SEM images of $\text{Mg}_2(m\text{-dobdc})\text{-ST}$ (left) and $\text{Mg}_2(m\text{-dobdc})\text{-MC}$ (right).

preparation of $\text{Mg}_2(\text{dobdc})$, such as employing $\text{Mg}(\text{OAc})_2 \cdot 4\text{H}_2\text{O}$ as a basic Mg precursor, were tested as well.^{22–24} Characterization of the produced solids by powder X-ray diffraction (PXRD)²⁵ validated that combining $\text{H}_4m\text{-dobdc}$ and $\text{Mg}(\text{NO}_3)_2 \cdot 6\text{H}_2\text{O}$ in 1:1 DMF:MeOH (0.03 M) at 120 °C for 48 h was optimal to yield highly crystalline $\text{Mg}_2(m\text{-dobdc})\text{-ST}$ (Fig. 3, ESI† Fig. S5). This synthesis can be readily scaled to produce $\text{Mg}_2(m\text{-dobdc})\text{-ST}$ on at least 0.5 g scale (Fig. 3, ESI† Fig. S6) and is reproducible as well (ESI† Fig. S17). Soaking the resulting MOF in DMF at 120 °C to remove residual starting materials, then in MeOH at 60 °C to remove DMF, and then in acetone at room temperature to remove MeOH, was sufficient to remove coordinating solvents and soluble impurities from $\text{Mg}_2(m\text{-dobdc})\text{-ST}$, as confirmed by acid digestion and analysis of the resulting solution by ^1H NMR (ESI† Fig. S13). Unfortunately, higher reaction concentrations (>0.1 M) led to impure materials (not shown), limiting the scalability of this solvothermal method.²⁶

Having optimized the solvothermal synthesis of $\text{Mg}_2(m\text{-dobdc})$, we set out to improve the mechanochemical synthesis of this material for comparison. Previously, we reported the mechanochemical synthesis of $\text{Mg}_2(\text{dobdc})$ using N,N -diisopropylethylamine (Hünig's base) as both the base required to deprotonate the linker precursor and as the liquid to facilitate liquid-assisted grinding in a planetary ball mill.¹⁴ This method could be generalized to the synthesis of porous $\text{Mg}_2(m\text{-dobdc})$ with modest crystallinity. We hypothesized that careful optimization of the Mg precursor ($\text{Mg}(\text{NO}_3)_2 \cdot 6\text{H}_2\text{O}$, $\text{Mg}(\text{OAc})_2 \cdot 4\text{H}_2\text{O}$, or MgO), base (Hünig's base, Et_3N , or 2,6-lutidine), and grinding time (1, 5, or 10 min) would enable the synthesis of $\text{Mg}_2(m\text{-dobdc})\text{-MC}$ with

maximum crystallinity and porosity (see ESI† section 4 for details). Indeed, the combination of $\text{Mg}(\text{NO}_3)_2 \cdot 6\text{H}_2\text{O}$, Et_3N , and 5–10 min grinding time was optimal to yield crystalline $\text{Mg}_2(m\text{-dobdc})\text{-MC}$ (Fig. 4, ESI† Fig. S18 and S19). This method could be reproducibly carried out with 10 min of grinding at 600 rpm to produce $\text{Mg}_2(m\text{-dobdc})\text{-MC}$ on 0.5 g scale in excellent yield (Fig. 3, ESI† Fig. S20 and S31). Notably, this mechanochemical synthesis bypasses the use of toxic DMF,²⁷ representing a green alternative to the solvothermal synthesis of $\text{Mg}_2(m\text{-dobdc})\text{-ST}$. No MOF was obtained with 2,6-lutidine, likely because it is not basic enough to fully deprotonate $\text{H}_4m\text{-dobdc}$.

With optimized samples of $\text{Mg}_2(m\text{-dobdc})\text{-ST}$ and $\text{Mg}_2(m\text{-dobdc})\text{-MC}$ in hand, we compared their crystallite morphologies (Fig. 5) and porosities (Table 1) in order to understand how synthesis procedure affects the physical properties of $\text{Mg}_2(m\text{-dobdc})$. Characterization of $\text{Mg}_2(m\text{-dobdc})\text{-ST}$ by scanning electron microscopy (SEM) revealed that it is composed of crystalline needles >5 μm in length on average (Fig. 5 left, ESI† Fig. S12). A needle-like morphology for $\text{Mg}_2(m\text{-dobdc})\text{-ST}$ is consistent with that previously reported for single crystals of the isostructural framework $\text{Co}_2(m\text{-dobdc})$.^{25,28} Similarly, $\text{Mg}_2(m\text{-dobdc})\text{-MC}$ is comprised of needles <1 μm in length (Fig. 5, right, ESI† Fig. S26). The smaller crystallites for mechanochemically synthesized $\text{Mg}_2(m\text{-dobdc})\text{-MC}$ likely arise due to rapid deprotonation of $\text{H}_4m\text{-dobdc}$ by triethylamine during the reaction.^{14,29}

Careful activation of $\text{Mg}_2(m\text{-dobdc})\text{-ST}$ and $\text{Mg}_2(m\text{-dobdc})\text{-MC}$ under high vacuum (<10 μbar) at 180 °C for at least 24 h was sufficient to fully remove solvent molecules from both frameworks. Their porosities were assessed by collecting 77 K N_2 adsorption isotherms (ESI† Fig. S9 and S23). As expected, $\text{Mg}_2(m\text{-dobdc})\text{-ST}$ and $\text{Mg}_2(m\text{-dobdc})\text{-MC}$ are both microporous, with BET and Langmuir surface areas comparable to those reported for related $\text{Mg}_2(\text{dobdc})$ (Table 1).^{10,12} The BET surface area of $\text{Mg}_2(m\text{-dobdc})\text{-MC}$ (1653 ± 2 $\text{m}^2 \text{g}^{-1}$) is somewhat higher than that of $\text{Mg}_2(m\text{-dobdc})\text{-ST}$ (1556 ± 2), reflecting a greater degree of accessible pores and/or the presence of insoluble, amorphous impurities in the latter material. We note that heating $\text{Mg}_2(m\text{-dobdc})$ with

Table 1 77 K N_2 BET and Langmuir surface areas of $\text{Mg}_2(m\text{-dobdc})\text{-ST}$ and $\text{Mg}_2(m\text{-dobdc})\text{-MC}$. Literature values reported for related $\text{Mg}_2(\text{dobdc})$ are included for comparison

Material	BET surface area ($\text{m}^2 \text{g}^{-1}$)	Langmuir surface area ($\text{m}^2 \text{g}^{-1}$)
$\text{Mg}_2(m\text{-dobdc})\text{-ST}$	1556 ± 2	1971 ± 3
$\text{Mg}_2(m\text{-dobdc})\text{-MC}$	1653 ± 2	1964 ± 38
$\text{Mg}_2(\text{dobdc})$	1495 (ref. 12)	1905–1957 (ref. 10 and 12)



Fig. 6 30 °C, 40 °C, and 50 °C CO₂ and 40 °C N₂ adsorption isotherms in a) $\text{Mg}_2(m\text{-dobdc})\text{-ST}$ and b) $\text{Mg}_2(m\text{-dobdc})\text{-MC}$. The lines correspond to individual fits to the dual-site Langmuir model. A data point was considered equilibrated when <0.01% pressure change occurred over a 30 s interval. c) Enthalpy of adsorption ($-\Delta H_{\text{ads}}$) values for $\text{Mg}_2(m\text{-dobdc})\text{-ST}$ and $\text{Mg}_2(m\text{-dobdc})\text{-MC}$ determined using simultaneous fits to dual-site Langmuir models. d) Summary of CO₂ and N₂ uptake values and non-competitive CO₂/N₂ selectivities relevant to CO₂ capture from coal flue gas for $\text{Mg}_2(m\text{-dobdc})\text{-ST}$ and $\text{Mg}_2(m\text{-dobdc})\text{-MC}$. The corresponding values for $\text{Mg}_2(\text{dobdc})$ reported in the literature are included for reference.¹⁹

ramp rates faster than 1 °C min⁻¹ or to temperatures greater than 180 °C consistently led to lower surface areas, likely due to partial pore collapse. Nonetheless, these findings confirm that highly porous and crystalline $\text{Mg}_2(m\text{-dobdc})$ can be readily prepared under both solvothermal and mechanochemical conditions.

Given the microporosity of both $\text{Mg}_2(m\text{-dobdc})$ samples and the high capacities of closely related $\text{Mg}_2(\text{dobdc})$ for a range of adsorbates,^{10,12} we assessed the potential suitability of $\text{Mg}_2(m\text{-dobdc})\text{-ST}$ and $\text{Mg}_2(m\text{-dobdc})\text{-MC}$ for gas capture applications using CO₂ scrubbing from coal flue gas as a representative separation. As such, CO₂ adsorption and desorption isotherms at 30 °C, 40 °C, and 50 °C and N₂ adsorption and desorption isotherms at 40 °C were collected for $\text{Mg}_2(m\text{-dobdc})\text{-ST}$ (Fig. 6a, ESI† Fig. S14 and S15) and $\text{Mg}_2(m\text{-dobdc})\text{-MC}$ (Fig. 6b, ESI† Fig. S28 and S29). In all cases, gas sorption was found to be completely reversible. Both materials exhibit steep uptake at low CO₂ pressures, indicative of strong interaction of CO₂ with exposed Mg(II)

sites.¹² The maximum CO₂ uptakes for both materials at 30 °C and 1 bar of CO₂ are 6.50 mmol g⁻¹ for $\text{Mg}_2(m\text{-dobdc})\text{-ST}$ and 8.69 mmol g⁻¹ for $\text{Mg}_2(m\text{-dobdc})\text{-MC}$; the latter value is similar to that predicted for binding one CO₂ per Mg(II) site in this material (8.24 mmol g⁻¹). The higher CO₂ capacity of $\text{Mg}_2(m\text{-dobdc})\text{-MC}$ than $\text{Mg}_2(m\text{-dobdc})\text{-ST}$ is consistent with its higher 77 K N₂ BET surface area and suggests that the mechanochemically synthesized MOF has more accessible Mg(II) sites.

To confirm that CO₂ binding in $\text{Mg}_2(m\text{-dobdc})$ materials likely occurs at coordinatively unsaturated Mg(II) sites, the CO₂ adsorption isotherms were fit using dual-site Langmuir models both independently and simultaneously (ESI† Tables S2 and S4). The independent dual-site Langmuir model fits are included in Fig. 6a and b and represent good fits to the experimental data. Using the Clausius–Clapeyron relationship, the differential enthalpies of adsorption ($-\Delta H_{\text{ads}}$) as a function of CO₂ loading were calculated (Fig. 6c, ESI† Fig. S16 and S30). The $-\Delta H_{\text{ads}}$ values at low coverage

are comparable for $\text{Mg}_2(m\text{-dobdc})\text{-MC}$ (42 kJ mol⁻¹) and $\text{Mg}_2(m\text{-dobdc})\text{-ST}$ (37 kJ mol⁻¹) and are similar to those previously reported for CO₂ adsorption in MOFs bearing accessible Mg(II) sites as well (38–43 kJ mol⁻¹).^{10,30} The $-\Delta H_{\text{ads}}$ plots support that $\text{Mg}_2(m\text{-dobdc})\text{-MC}$ contains more accessible Mg(II) sites than $\text{Mg}_2(m\text{-dobdc})\text{-ST}$, as the strong binding of CO₂ drop offs at higher loadings in this material (~ 0.7 CO₂ per Mg vs. ~ 0.4 CO₂ per Mg in $\text{Mg}_2(m\text{-dobdc})\text{-ST}$).

Among MOFs, $\text{Mg}_2(\text{dobdc})$ possesses one of the highest reported CO₂ capacities (5.28 mmol g⁻¹) under conditions relevant to CO₂ capture from coal flue gas (150 mbar, 40 °C) (Fig. 6d).^{10,18,19} Coupled with minimal uptake of N₂ at 750 mbar and 40 °C (0.50 mmol g⁻¹),¹⁹ this high CO₂ uptake at low pressures makes $\text{Mg}_2(\text{dobdc})$ a promising material for CO₂/N₂ separations. While the CO₂ uptake of $\text{Mg}_2(m\text{-dobdc})\text{-ST}$ at 150 mbar and 40 °C (3.99 mmol g⁻¹) is less than that reported for $\text{Mg}_2(\text{dobdc})$, likely due to its dearth of accessible Mg(II) sites, $\text{Mg}_2(m\text{-dobdc})\text{-MC}$ exhibits a higher capacity for CO₂ (6.14 mmol g⁻¹) than $\text{Mg}_2(\text{dobdc})$ under these conditions (Fig. 6d). Previous studies have suggested that the metal centers of $\text{M}_2(m\text{-dobdc})$ MOFs are slightly more Lewis acidic than those of $\text{M}_2(\text{dobdc})$ MOFs,¹³ which may account for the enhanced CO₂ uptake at low pressures in $\text{Mg}_2(m\text{-dobdc})\text{-MC}$. Consistently, the N₂ capacity of $\text{Mg}_2(m\text{-dobdc})\text{-MC}$ at 750 mbar and 40 °C (0.89 mmol g⁻¹) is higher than that reported for $\text{Mg}_2(\text{dobdc})$ as well. Given the unclear suitability of calculating selectivities in open metal site MOFs using ideal adsorbed solution theory (IAST),³¹ we elected to calculate non-competitive CO₂/N₂ selectivities under conditions relevant to coal flue gas capture for $\text{Mg}_2(m\text{-dobdc})\text{-ST}$, $\text{Mg}_2(m\text{-dobdc})\text{-MC}$, and $\text{Mg}_2(\text{dobdc})$ instead (Fig. 6d). The non-competitive CO₂/N₂ selectivity calculated for $\text{Mg}_2(\text{dobdc})$ is the highest (53),¹⁹ followed by $\text{Mg}_2(m\text{-dobdc})\text{-ST}$ (44), and then $\text{Mg}_2(m\text{-dobdc})\text{-MC}$ (35). The diminished non-competitive CO₂/N₂ selectivity for $\text{Mg}_2(m\text{-dobdc})\text{-MC}$ is due to the higher uptake of N₂ in this material. Nonetheless, these findings support that $\text{Mg}_2(m\text{-dobdc})\text{-MC}$ is competitive with the widely studied MOF $\text{Mg}_2(\text{dobdc})$ for this representative separation. Further, the superior gas sorption performance of $\text{Mg}_2(m\text{-dobdc})\text{-MC}$ over $\text{Mg}_2(m\text{-dobdc})\text{-ST}$ indicates that mechanochemical methods may be preferable for the scalable synthesis of this framework.

Conclusions

Owing to their low cost and high gravimetric gas storage capacities, MOFs bearing high densities of coordinatively unsaturated Mg(II) centers are highly sought after. We have demonstrated that $\text{Mg}_2(m\text{-dobdc})$ synthesized under mechanochemical conditions is a promising new Mg-based MOF due to its strong binding and high capacity for CO₂ at low pressures. Notably, the work presented herein represents a rare example in which a mechanochemically synthesized MOF displays superior gas sorption properties compared to material synthesized under traditional solvothermal conditions.^{14–17} Moving forward,

mechanochemical methods will prove to be a valuable alternative to solvothermal syntheses for the preparation of high-quality MOFs for applications in gas storage, chemical separations, and drug delivery.

Author contributions

P. J. M. and R. M. M. conceived the project. E. Y. C. and R. M. M. carried out all experiments. The manuscript was written through the contributions of all authors, and all authors approved of the final version.

Conflicts of interest

P. J. M. is listed as an inventor on several patents related to the application of MOFs for gas capture.

Acknowledgements

The development of new methods for the synthesis of Mg-based MOFs was supported by the National Institute of General Medical Sciences of the National Institutes of Health under award number R35GM138165. The content is solely the responsibility of the authors and does not necessarily represent the official views of the National Institutes of Health. The characterization of the CO₂ adsorption properties of $\text{Mg}_2(m\text{-dobdc})$ was supported by the U.S. Department of Energy, Office of Science, Office of Basic Energy Sciences under award number DE-SC0021000. This work made use of the Cornell Center for Materials Research Shared Facilities, which are supported through the NSF MRSEC program (DMR-1719875). Some of the ¹H NMR data in this work were collected on a Bruker INOVA 500 MHz spectrometer that was purchased with support from the NSF (CHE-1531632). We thank Cornell University for providing a Summer Experience Grant to E. Y. C.

Notes and references

- H. Furukawa, K. E. Cordova, M. O'Keeffe and O. M. Yaghi, *Science*, 2013, **341**, 1230444.
- Y. Sun, L. Zheng, Y. Yang, X. Qian, T. Fu, X. Li, Z. Yang, H. Yan, C. Cui and W. Tan, *Nano-Micro Lett.*, 2020, **12**, 103.
- A. Bavykina, N. Kolobov, I. S. Khan, J. A. Bau, A. Ramirez and J. Gascon, *Chem. Rev.*, 2020, **120**, 8468–8535.
- H. Li, K. Wang, Y. Sun, C. T. Lollar, J. Li and H.-C. Zhou, *Mater. Today*, 2018, **21**, 108–121.
- C. A. Trickett, A. Helal, B. A. Al-Maythaly, Z. H. Yamani, K. E. Cordova and O. M. Yaghi, *Nat. Rev. Mater.*, 2017, **2**, 17045.
- Ü. Kökçam-Demir, A. Goldman, L. Esrafil, M. Gharib, A. Morsali, O. Weingart and C. Janiak, *Chem. Soc. Rev.*, 2020, **49**, 2751–2798.
- N. L. Rosi, J. Kim, M. Eddaoudi, B. Chen, M. O'Keeffe and O. M. Yaghi, *J. Am. Chem. Soc.*, 2005, **127**, 1504–1518.
- M. E. Zick, J.-H. Lee, M. I. Gonzalez, E. O. Velasquez, A. A. Uliana, J. Kim, J. R. Long and P. J. Milner, *J. Am. Chem. Soc.*, 2021, **143**, 1948–1958.

- 9 À. Ruyra, A. Yazdi, J. Espín, A. Carné-Sánchez, N. Roher, J. Lorenzo, I. Imaz and D. Maspoch, *Chem. – Eur. J.*, 2015, **21**, 2508–2518.
- 10 W. L. Queen, M. R. Hudson, E. D. Bloch, J. A. Mason, M. I. Gonzalez, J. S. Lee, D. Gygi, J. D. Howe, K. Lee and T. A. Darwish, *Chem. Sci.*, 2014, **5**, 4569–4581.
- 11 T. Grant Glover, G. W. Peterson, B. J. Schindler, D. Britt and O. Yaghi, *Chem. Eng. Sci.*, 2011, **66**, 163–170.
- 12 S. R. Caskey, A. G. Wong-Foy and A. J. Matzger, *J. Am. Chem. Soc.*, 2008, **130**, 10870–10871.
- 13 M. T. Kapelewski, S. J. Geier, M. R. Hudson, D. Stück, J. A. Mason, J. N. Nelson, D. J. Xiao, Z. Hulvey, E. Gilmour, S. A. FitzGerald, M. Head-Gordon, C. M. Brown and J. R. Long, *J. Am. Chem. Soc.*, 2014, **136**, 12119–12129.
- 14 Z. Wang, Z. Li, M. Ng and P. J. Milner, *Dalton Trans.*, 2020, **49**, 16238–16244.
- 15 D. Chen, J. Zhao, P. Zhang and S. Dai, *Polyhedron*, 2019, **162**, 59–64.
- 16 J. L. Howard, Q. Cao and D. L. Browne, *Chem. Sci.*, 2018, **9**, 3080–3094.
- 17 T. Friščić, in *Encyclopedia of Inorganic and Bioinorganic Chemistry*, John Wiley & Sons, Ltd, 2014, pp. 1–19.
- 18 E. J. Granite and H. W. Pennline, *Ind. Eng. Chem. Res.*, 2002, **41**, 5470–5476.
- 19 J. A. Mason, K. Sumida, Z. R. Herm, R. Krishna and J. R. Long, *Energy Environ. Sci.*, 2011, **4**, 3030.
- 20 A. Modak and S. Jana, *Microporous Mesoporous Mater.*, 2019, **276**, 107–132.
- 21 Y. Sadamitsu, A. Okumura, K. Saito and T. Yamada, *Chem. Commun.*, 2019, **55**, 9837–9840.
- 22 K. A. Colwell, M. N. Jackson, R. M. Torres-Gavosto, S. Jawahery, B. Vlasisavljevich, J. M. Falkowski, B. Smit, S. C. Weston and J. R. Long, *J. Am. Chem. Soc.*, 2021, **143**, 5044–5052.
- 23 L. Garzón-Tovar, A. Carné-Sánchez, C. Carbonell, I. Imaz and D. Maspoch, *J. Mater. Chem. A*, 2015, **3**, 20819–20826.
- 24 D. J. Tranchemontagne, J. R. Hunt and O. M. Yaghi, *Tetrahedron*, 2008, **64**, 8553–8557.
- 25 J. E. Bachman, M. T. Kapelewski, D. A. Reed, M. I. Gonzalez and J. R. Long, *J. Am. Chem. Soc.*, 2017, **139**, 15363–15370.
- 26 D. R. Du Bois, K. R. Wright, M. K. Bellas, N. Wiesner and A. J. Matzger, *Inorg. Chem.*, 2022, **61**, 4550–4554.
- 27 F. P. Byrne, S. Jin, G. Paggiola, T. H. M. Petchey, J. H. Clark, T. J. Farmer, A. J. Hunt, C. Robert McElroy and J. Sherwood, *Sustainable Chem. Processes*, 2016, **4**, 7.
- 28 M. I. Gonzalez, M. T. Kapelewski, E. D. Bloch, P. J. Milner, D. A. Reed, M. R. Hudson, J. A. Mason, G. Barin, C. M. Brown and J. R. Long, *J. Am. Chem. Soc.*, 2018, **140**, 3412–3422.
- 29 G. Ayoub, B. Karadeniz, A. J. Howarth, O. K. Farha, I. Dilović, L. S. Germann, R. E. Dinnebie, K. Užarević and T. Friščić, *Chem. Mater.*, 2019, **31**, 5494–5501.
- 30 P. J. Milner, J. D. Martell, R. L. Siegelman, D. Gygi, S. C. Weston and J. R. Long, *Chem. Sci.*, 2018, **9**, 160–174.
- 31 R. Krishna and J. M. van Baten, *ACS Omega*, 2021, **6**, 15499–15513.